VNU Journal of Science: Mathematics - Physics

Journal homepage: https://js.vnu.edu.vn/MaP

Original Article

Investigation of Thermal and ultrasonic properties of (Mg_2La, Mg_2Nd, Mg_2Sm) (C14) Phase of Intermetallic Compound

Riya Singh[1,*], Giridhar Mishra[1,2], Ramanshu P. Singh[1]

[1]*Institute of Physical Sciences for Study and Research, Veer Bahadur Singh Purvanchal University, Jaunpur-222003, India*

[2]*Interdisciplinary Centre for Water and Energy Research, Veer Bahadur Singh Purvanchal University, Jaunpur-222003, India*

Received 24th November 2025
Revised 16th December 2025; Accepted 9th April 2026

Abstract: In this study, the physical characteristics of the hexagonal closed-packed structure's Mg_2La, Mg_2Nd, and Mg_2Sm (C14) phases at 300 K have been examined. The L-J potential approach was used to compute SOECs and TOECs. The obtained SOECs and TOECs are utilized to assess mechanical characteristics at various angles along the unique axis. Thermophysical properties of the material at 300K have been evaluated, such as energy density, thermal conductivity, Debye temperature, and Debye average velocity of selected materials. Beyond this, we have computed the ultrasonic acoustic coupling constant at room temperature. Ultimately, the thermoelastic relaxation process and phonon-phonon interaction are used to obtain attenuation. The obtained results have been compared with previous research on similar kinds of HCP metal.

Keywords: Mg_2La, Mg_2Nd, and Mg_2Sm (C14) Phase intermetallic compound, Debye temperature, ultrasonic properties, thermal conductivity.

1. Introduction

Magnesium-containing alloys are optimistic materials with many advantages in different areas, including the aerospace industry, automobiles, and microstructure [1]. Almost all magnesium alloys contain intermetallic compounds. They can arise by solid-state transitions at low temperatures or precipitate during casting at high temperatures. The precise ternary addition and cooling rate during

* Corresponding author (s).
E-mail address: riyafeb44@gmail.com

https://doi.org/10.25073/2588-1124/vnumap.5097

solidification can result in various intermetallic morphologies, notably, needle-like, lamellar, Chinese calligraphy, rosette-like, blocky, and more. They range in size from nanometres to micrometres. Magnesium-based intermetallic compounds are essential for improved mechanical and microstructural characteristics [2]. Mg-RE alloys have a weaker basal-type texture, defined by the basal poles' expansion towards the sheet rolling direction (RD), giving rise to the so-called r-type texture. In contrast, sheets of pure magnesium and ordinary magnesium alloys frequently have a strong basal texture. It was demonstrated that structural magnesium alloys can benefit from the addition of Y and specific rare earth (RE) elements like Ce. These consequences include a rise in room-temperature ductility and a weakening of texture [3]. Thus, a precise theoretical knowledge of the Mg-Nd alloy is required." This paper gives information about the structural and electrical characteristics of selected materials, which was examined by the Lennard-Jones potential model. The element Nd is a primary example of a rare earth metal. It is well known that adding Nd to magnesium alloy increases the solid-solution strengthening. The amount of Nd added was found to enhance the time it takes for age hardening and creep resistance [4]. Mg_2Nd has several types of crystal structure, such as HCP, FCC, DHCP, and CBCO, for c-axis base-centered orthorhombic also exhibits an HCP structure stable at room temperature. At 548 °C, Nd has a maximum solubility of almost 3.7 weight percent, and at 300 °C, it steadily drops to nearly zero. Despite the intricate and contentious precipitation patterns discussed by the researchers, the Mg-Nd has demonstrated robust precipitation hardening, with $Mg_{41}Nd_5$ being the equilibrium phase. At the eutectic temperature of 595 °C, Ce solubility in Mg reaches its maximum of 0.8 weight percent, however, it quickly drops to nearly zero at 300 K.

Similar to the Mg-Nd formation, the precipitates that form in the Mg-Ce binary system after age-hardening; however, the strength is comparatively low due to Ce's low solid solubility in Mg [5].

2. Theory of Elastic Constants and Moduli

For the HCP structured Mg_2La, Mg_2Nd, and Mg_2Sm (C14) phase, SOECs and TOECs have been utilized the L-J potential model for evaluation. The interaction potential φ(r), which is given by the equation and stated in terms of the constants (a_0 and b_0) and integers (m and n) [6].

$$\phi(r) = -\frac{a_0}{r^m} + \frac{b_0}{r^n} \tag{1}$$

It provides equations for the creation of six SOECs and ten TOECs.

$$\begin{aligned}
C_{11} &= 24.1p^4C' & C_{111} &= 126.9p^2B + 8.853p^4C' \\
C_{13} &= 1.925p^6C' & C_{112} &= 19.168p^2B - 1.61p^4C' \\
C_{33} &= 3.464p^8C' & C_{113} &= 1.924p^4B + 1.155p^4C' \\
C_{44} &= 2.309p^4C' & C_{123} &= 1.617p^4B - 1.155p^6C' \\
C_{66} &= 9.851p^4C' & C_{133} &= 3.695p^6B \\
C_{12} &= 5.918p^4C' & C_{155} &= 1.539p^4B \\
 & & C_{144} &= 2.309p^4B \\
 & & C_{344} &= p^6B \\
 & & C_{222} &= 101.039p^2B + 9.007p^2C' \\
 & & C_{333} &= 5.196p^8B
\end{aligned} \tag{2}$$

Where, $p = c/a$, $C' = x\frac{a}{p^5}$, $x = \frac{1}{8}\left[\frac{nb_{0(n-m)}}{(a^{n+4})}\right]$

$B = \psi \frac{a^3}{p^3}$, and $\psi = -\frac{x}{6a^2(m+n+6)}$ Indicate (m, n) integers, b_0 stand for L-J potential. Using the Voigt-Reuss-Hill method, SOECs were acclimated to acquire the importance of physical parameters, including the material's (B), (G), (Y), (σ), and (B/G) [7]. Physical quantities are determined by following expression [8].

$$\left.\begin{aligned} B_R = \frac{C^2}{M}\ ; \quad B_V = \frac{2(C_{11}+C_{12})+4C_{13}+C_{33})}{9}\ ; B = \frac{B_V+B_R}{2}\ ; \quad \mathrm{Y} = \frac{9GB}{G+3B} \\ G_V = \frac{M+12(C_{44}+C_{66})}{30}\ ; G_R = \frac{5C^2C_{44}C_{66}}{2[3B_VC_{44}C_{66}+C^2(C_{44}+C_{66})}; G = \frac{G_V+G_R}{2}\ ; \\ \sigma = \frac{3B-2G}{2(3B+G)} \\ M = C_{11}+C_{12}+2C_{33}-4C_{13}; \\ C^2 = (C_{11}+C_{12})C_{33}-4C_{13}+C_{13}^2; \end{aligned}\right\} \quad (3)$$

Where, G_V and G_R Voigt and Reuss shear constants [9]. The brittleness and ductility of the solids can be inferred from Pugh's ratio $(k') = B/G$.

3. Theory of Ultrasonic Velocity

Three-direction-dependent ultrasonic waves are present in hcp materials, propagating in different directions [10]. In these modes, the ultrasonic wave velocity can be calculated using the material density and second-order elastic constant. When propagating in a hexagonal-close-packed structure, the ultrasonic velocity is determined by the following equations [11].

$$V_L^2 = \frac{\left[C_{33}cos^2\theta + C_{11}sin^2\theta + C_{44} + \left\{\left(C_{11}sin^2\theta - C_{33}cos^2\theta + C_{44}(cos^2\theta - sin^2\theta)\right)^2 + 4cos^2\theta sin^2\theta(C_{13}+C_{44})^2\right\}^{1/2}\right]}{2\rho} \quad (4)$$

$$V_{S1}^2 = \frac{\left[C_{33}cos^2\theta + C_{11}sin^2\theta + C_{44} - \left\{\left(C_{11}sin^2\theta - C_{33}cos^2\theta + C_{44}(cos^2\theta - sin^2\theta)\right)^2 + 4cos^2\theta sin^2\theta(C_{13}+C_{44})^2\right\}^{1/2}\right]}{2\rho} \quad (5)$$

$$V_{S2}^2 = \frac{[C_{44}cos^2\theta + C_{166}sin^2\theta]}{\rho} \quad (6)$$

Here, V_{S1} quasi-shear velocity, V_{S2} shear velocity , and V_L longitudinal velocity.
θ and ρ angle with the unique axis of the crystal and density of material, respectively.
The following formula can be used to get the Debye average velocity for a hexagonal-structured crystal along any angle with a unique axis:[12]

$$V_D = \left[\frac{1}{3}\left(\frac{1}{V_L^3} + \frac{1}{V_{S1}^3} + \frac{1}{V_{S2}^3}\right)\right]^{-1/3} \quad (7)$$

4. Theory of Ultrasonic Attenuation

Physical characteristics are connected to attenuation in solids and liquids. At high temperatures, Akhiezer loss and loss from thermo-elastic relaxation are the two prime causes of attenuation in materials [13].

$$(\alpha/f^2)_{Akh} = \frac{4\pi^2\tau E_0(D/3)}{2\rho V^3} \tag{8}$$

The thermal relaxation time denoted by τ, amount of time required to get the thermal phonons back into equilibrium, as stated by the following formula [14].

$$\tau = \tau_S = \frac{\tau_L}{2} = \frac{3k}{C_v V_D^2} \tag{9}$$

Here, specific heat per unit volume C_v and thermal conductivity k , (τ_s , τ_L) are thermal relaxation time. This equation used to determine by thermoelastic loss $(\alpha/f^2)_{Th}$ [15].

$$(\alpha/f^2)_{Th} = 4\pi^2 < \gamma_i^j >^2 \frac{kT}{2\rho V_L^5} \tag{10}$$

5. Results and Discussion

The lattice parameters (a, c) for the Mg_2La, Mg_2Nd, and Mg_2Sm (C14) Phase at ambient temperature (300 K), and axial ratio (p) are 6.237(Å), 10.056(Å), 6.162(Å), 9.967(Å), 6.121(Å), 9.888(Å) and 1.61, 1.61, 1.61 respectively [1]. The computed values for the second and third-order elastic constants are exhibited in Table 1.

Table1. SOECs and TOECs elastic constants for (C14) phase at ambient temperature 300 K (GPa).

Material	C_{11}	C_{12}	C_{13}	C_{33}	C_{44}	C_{66}
Mg_2La	59.1	14.5	12.2	57.1	14.7	22.3
Mg_2Nd	72.6	17.8	15	70.1	18	27.4
Mg_2Sm	76.7	18.8	15.9	74	19	28.9

Material	C_{111}	C_{112}	C_{113}	C_{123}	C_{133}	C_{344}	C_{144}	C_{155}	C_{222}	C_{333}
Mg_2La	-97	-31	-15	-40	-19	-18	-46	-31	-76	-70
Mg_2Nd	-120	-39	-19	-49	-24	-22	-57	-38	-94	-86
Mg_2Sm	-130	-41	-20	-52	-25	-23	-60	-40	-99	-91

Table2. Mechanical properties (B, G, Y,ϑ) at 300K (GPa).

	The Present work				Other Studies			
Material	B	G	Y	$\boldsymbol{\vartheta}$	B	G	Y	$\boldsymbol{\vartheta}$
Mg_2La	28.1	9	26.1	0.3451	35.23	13.70	36.38	0.32
Mg_2Nd	34.5	11.9	32.1	0.3451	38.78	17.14	44.83	0.30
Mg_2Sm	36.5	12.6	33.9	0.3451	40.53	19.00	49.31	0.29

Table 1. shows that the selected material for SOECs and TOECs is mechanically stable. For a hexagonal crystal, Born stability conditions are also satisfied. i.e. [1].

$$C_{44} > 0,\ C_{11} > |C_{12}|, (C_{11} + 2C_{12})C_{33} > 2C_{13}^2$$

The intermetallic compound has been confirmed to be mechanically stable. As shown in Table 1, SOECs and TOECs are reasonable [1]. The bulk modulus and stiffness of the material are interconnected to one another, which justifies the current second-order elastic constants of the selected material under the potential model method.

As discussed in Table 2, the chosen materials are mechanically stable. For Mg_2La, the (B), (G), and (Y) at 300K are 28.1, 9, and 26.1(in GPa), respectively, which align with the values reported in the literature. Using the Voigt-Reuss-Hill method, the (B), (G), (Y), and Poisson's ratios have been computed. For Mg_2Nd (B), (G), and (Y) at 300K are 34.5, 11.9, and 32.1(in GPa), respectively, which also aligns well with previous literature. For Mg_2Sm, (B), (G), and (Y) at 300K are 36.5, 12.6, and 33.9(in GPa), respectively, which also agree well with other works of literature. Mg_2Sm exhibits higher elastic moduli compared to Mg_2Nd and Mg_2La. The current all-elastic moduli are consistent with the other studies, which show that the values are in Table 2, Comparison of elastic moduli Mg_2Sm has higher values than Mg_2Nd and Mg_2La. The present elastic moduli also show good agreement with other studies.

A material's stiffness is indicated by its Young's modulus, which gauges its resistance to uniaxial pressures. Shear stress and pressure can cause form changes, but the bulk and shear modulus show resistance to these changes. Information regarding the material's brittleness and ductility can be found using Pugh's and Poisson's ratios.

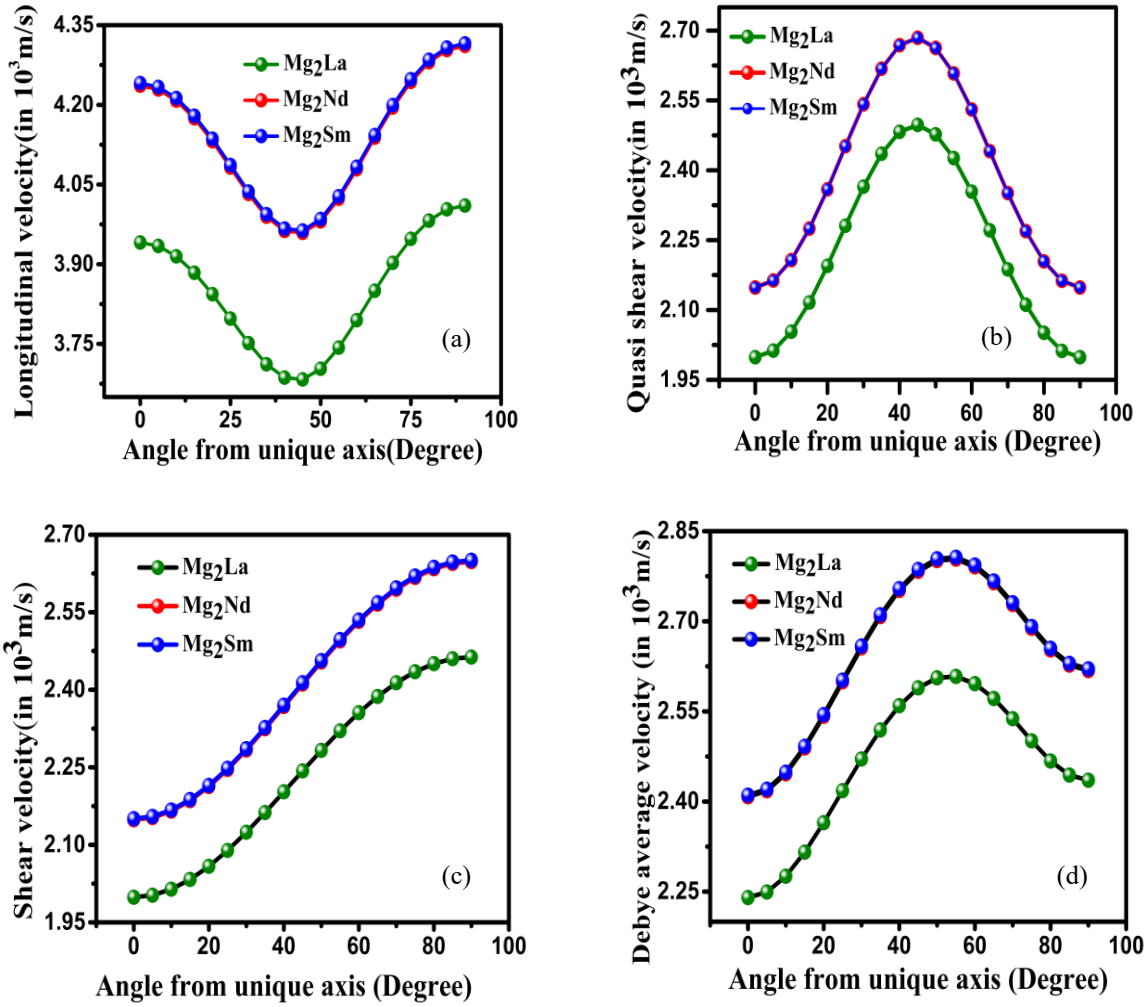

Figure 1. (a) (V_L), (b) (V_{s1}), (c) (V_{s2}), (d) (V_D) versus (θ) of Mg_2La, Mg_2Nd, and Mg_2Sm (C14) phase.

The ultrasonic velocities can be computed by the density of the material and the angle from the unique axis, for propagation at different orientations. Fig. 1 above displays the ultrasonic velocities V_L, V_{S1}, $V_{S2,}$ and V_D, as given in Figs. 1 (a to d).

For Mg_2Sm, the longitudinal wave velocity (V_L) decreases, but it also drops as the angle increases to 45°, With the particular axis before starting to get up again from 45° to 90°. Maximum velocity is 4.31×10^3m/s at an angle 90°. Mg_2Sm has a higher velocity in the analysis than Mg_2Nd and Mg_2La. As if, quasi shear wave velocity (V_{S1}) has the largest value of 2.68×10^3m/s at angle 45°. Shear velocity (V_{S2}) has a maximum value of 2.65×10^3m/s at an angle 90°. Debye average velocity (V_D) has a maximum value of 2.80×10^3m/s at an angle of 55°. The properties of Debye average velocity(V_D) are qualitatively the same as quasi-shear wave velocity. However, because they were not available in the literature, these velocities could not be confirmed. We could observe a reasonable agreement between the ultrasonic velocity measurements of the HCP intermetallic compound. Those angles that depend on velocity are found to be reasonable [16].

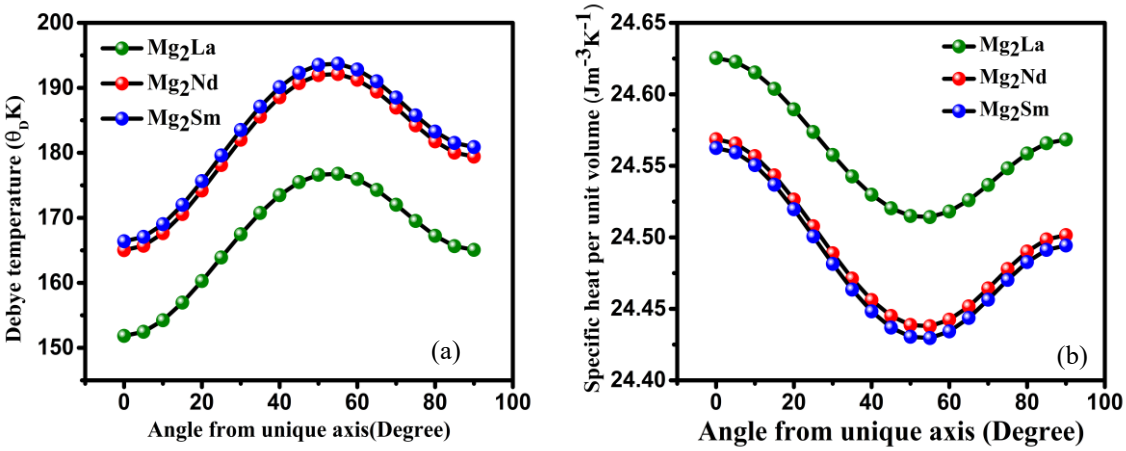

Figure 2. (a) (θ_D) ,(b) (C_v) versus (θ) of Mg_2La, Mg_2Nd, and Mg_2Sm (C14) Phase.

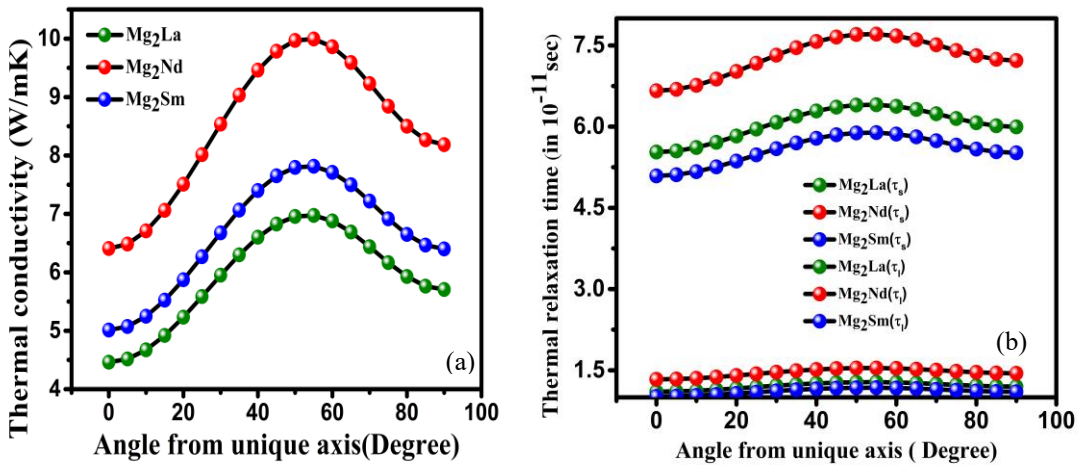

Figure 3. (a) (k), (τ_s, τ_l) versus (θ) of Mg_2La, Mg_2Nd, and Mg_2Sm (C14) Phase.

As described in Fig. 2, the specific heat per unit volume and the Debye temperature are opposite because of their inverse proportionality. Debye temperature admirers' equation, in the literature [17] and plotted in Fig. 2.

Fig 3. This implies that the thermal conductivity has the biggest impact on thermal relaxation time (τ) [18]. Thus, the calculated thermal relaxation time for the HCP structure of the chosen intermetallic compound at 300K is supported. A crucial component of material characterization is thermal conductivity, which can be assessed for the intermetallic compound. We can determine an equation from the literature [19].

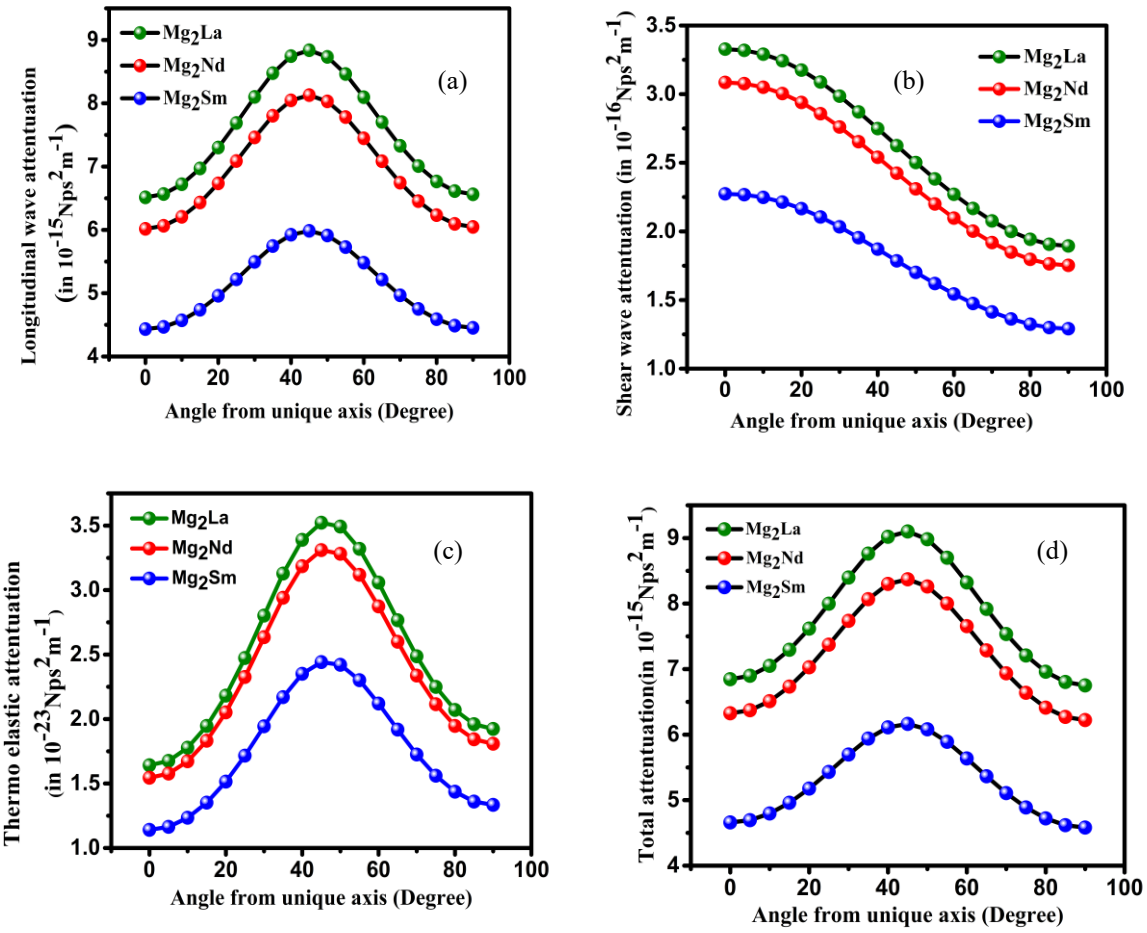

Figure 4. (a) (a/f_L^2), (b) (a/f_S^2) , (c) (a/f_{th}^2), (d) (a/f_{total}^2) versus (θ) of Mg_2La, Mg_2Nd, and Mg_2Sm(C14) phase.

This is due to a direct correlation between the material's thermoelastic characteristics and attenuation. Two forms of attenuation that are the subject of this study are thermoelastic relaxation and Akhiezer loss, which promoted by phonon-phonon interaction, and thermoelastic relaxation. Using Eq^n (10), and presented in Fig. 4, respectively, which has been used to evaluate the ultrasonic attenuations for Mg_2La, Mg_2Nd, and Mg_2Sm(C14) phases. In Fig. 4, the longitudinal wave attenuation is represented by the highest value of Mg_2La, and Shear wave attenuation, thermoelastic wave attenuation, and total

attenuation are the highest value of Mg_2La. From Fig.1, it is clear that the longitudinal velocity of Mg_2Sm is greater than Mg_2Nd, Mg_2La, and it reaches the maximum value 4.31×10^3m/s at an angle of 90°. Therefore, at room temperature, the phonon-phonon interaction mechanism dominates overall ultrasonic attenuation in Mg_2La, Mg_2Nd, and Mg_2Sm(C14) phase for the HCP structure. Regrettably, no prior experimental or theoretical information about the ultrasonic attenuations in Mg2La, Mg_2Nd, and Mg_2Sm(C14) phase has been described previously to allow for direct comparison and published to the best of our knowledge.

6. Conclusion

Our investigation's findings have led to the following significant conclusions.

Our findings are consistent with previous research, distinguished by the importance and significance of the L-J potential model. Mg_2Sm has further tensile strength and stiffness than Mg_2Nd and Mg_2La(C14) phase for the HCP structure. Specific heat per unit volume and Debye temperature are opposite because of their inverse proportionality. Thermal conductivity has the biggest impact on thermal relaxation time (τ) and the choice of material at 300K is supported. Pugh's ratio is shown in the ductility or brittleness. The ultrasonic attenuation in Mg_2La is higher than Mg_2Nd and Mg_2Sm(C14) phase at room temperature, the phonon-phonon interaction mechanism predominates above the thermoelastic loss in the selected materials. To further investigate the thermophysical properties of the Mg_2Sm, Mg_2Nd, and Mg_2La(C14) phase intermetallic compound, the outcomes will serve as a database.

Acknowledgement

The authors acknowledge the support from GSU grant under the PM-UShA scheme of the Government of India.

References

[1] S. Rameshkumar, G. Jaiganesh, V. Jayalakshmi, Structural, Phonon, Elastic, Thermodynamic And Electronic Properties of Mg–X (X = La, Nd, Sm) Intermetallics: The First Principles Study, J. Magnes. Alloy., Vol. 7, No. 1, 2019, pp. 166-185, https://doi.org/10.1016/j.jma.2018.12.003.

[2] N. Hort, Y. Huong, K. U. Kainer, Intermetallics in Magnesium Alloys, Adv. Eng. Mater., Vol. 8, No. 4, 2006, pp. 235-240, https://doi.org/10.1002/adem.200500202.

[3] S. Sandlöbes et al., Ductility Improvement of Mg Alloys By Solid Solution: Ab Initio Modeling, Synthesis and Mechanical Properties, Acta Mater., Vol. 70, 2014, pp. 92-104, https://doi.org/10.1016/j.actamat.2014.02.011.

[4] J. Z. Peng, Y. F. Wang, M. F. Gray, First-principles Study of Structural Stabilities and Electronic Properties of Mg-Nd Intermetallic Compounds, Phys. B Condens. Matter, Vol. 403, No. 13-16, 2008, pp. 2344-2348, https://doi.org/10.1016/j.physb.2007.12.016.

[5] J. M. Meier, J. Caris, A. A. Luo, Towards High Strength Cast Mg-RE Based Alloys: Phase Diagrams and Strengthening Mechanisms, J. Magnes. Alloy., Vol. 10, No. 6, 2022, pp. 1401-1427, https://doi.org/10.1016/j.jma.2022.03.008.

[6] C. P. Yadav, D. K. Pandey, D. Singh, Ultrasonic study of Laves phase compounds $ScOs_2$ and YOs_2, Indian J. Phys., Vol. 93, No. 9, 2019, pp. 1147-1153, https://doi.org/10.1007/s12648-019-01389-8.

[7] P. K. Yadawa, N. Chaurasiya, S. Rai, A. K. Prajapati, Temperature-Dependent Ultrasonic Properties of Semiconducting M_2CO_2 (M= Ti, Zr, Hf) MXenes, J. Sci. Res., Vol. 14, No. 3, 2022, pp. 735-748, https://doi.org/10.3329/jsr.v14i3.56976.

[8] A. K. Maddheshiya, N. Yadav, S. P. Singh, D. Singh, P. S. Yadav, R. R. Yadav, Mechanical, Elastic and Microstructural Investigations on HCP Phase High-Entropy Alloys, Mapan J. Metrol. Soc. India, Vol. 38, No. 4, 2023, pp. 1019-1026, https://doi.org/10.1007/s12647-023-00674-6.

[9] S. Tripathi, R. Agarwal, D. Singh, Size-Dependent Ultrasonic and Thermophysical Properties of Indium Phosphide Nanowires, Zeitschrift fur Naturforsch, Sect. A J. Phys. Sci., Vol. 75, No. 4, 2020, pp. 373-380, https://doi.org/10.1515/zna-2019-0351.

[10] A. K. Gupta, A. Gupta, S. Tripathi, V. Bhalla, J. M. Singh, Ultrasonic Properties of Hexagonal Closed Packed Metals, Univers. J. Mater. Sci., Vol. 1, No. 2, 2013, pp. 63-68, https://doi.org/10.13189/ujms.2013.010209.

[11] R. Srivastava, R. P. Singh, G. Mishra, Study of Mechanical and Thermophysical Properties of Ni3Ti, Zeitschrift fur Naturforsch, Sect. A J. Phys. Sci., 2024, https://doi.org/10.1515/zna-2024-0093.

[12] S. Tripathi, R. Agarwal, D. Singh, Size Dependent Elastic and Thermophysical Properties of Zinc Oxide Nanowires: Semiconductor Materials Characterisation for High Temperature Applications, Johnson Matthey Technol. Rev., Vol. 63, No. 3, 2019, pp. 166-176, https://doi.org/10.1595/205651319X15514400132039.

[13] B. Jyoti, S. P. Singh, M. Gupta, S. Tripathi, D. Singh, R. R. Yadav, Investigation of Zirconium Nanowire by Elastic, Thermal and Ultrasonic Analysis, Zeitschrift fur Naturforsch. - Sect. A J. Phys. Sci., Vol. 75, No. 12, 2020, pp. 1077-1084, https://doi.org/10.1515/zna-2020-0167.

[14] R. P. Singh, S. Yadav, G. Mishra, D. Singh, Pressure Dependent Ultrasonic Properties of Hcp Hafnium Metal, Zeitschrift fur Naturforsch, Sect. A J. Phys. Sci., Vol. 76, No. 6, 2021, pp. 549-557, https://doi.org/10.1515/zna-2021-0013.

[15] A. Singh, J. Bala, S. P. Singh, D. Singh, The Mechanical, Thermo-physical and Ultrasonic Properties of Scandium Nitride in B1 and B2 Phases, Vietnam J. Sci. Technol., Vol. 63, No. 1, 2025, pp. 161-175, https://doi.org/10.15625/2525-2518/20142.

[16] R. P. Singh, S. Yadav, A. Tiwari, Theoretical Investigation of Mechanical and Thermal Features in ScTiZr and ScTiHf Alloys: A Comparative Study, J. Pure Appl. Ultrason., Vol. 45, No. 11, 2023, pp. 50-59, http://dx.doi.org/10.1016/j.jpaa.2012.03.014.

[17] C. P. Yadav, D. K. Pandey, D. Singh, D. Singh, Ultrasonic Non-destructive Evaluation of w-GaSe at Different Temperatures, Nondestruct. Test. Eval., Vol. 40, No. 2, 2024, pp. 739-750, https://doi.org/10.1080/10589759.2024.2331258.

[18] A. Singh, D. Singh, S. Tripathi, R. Khenata, Impact of Alloying on Elastic, Thermal and Ultrasonic Properties of Wurtzite ScxAl1-xN, Phys. Lett. Sect. A Gen. At. Solid State Phys., Vol. 527, No. 9, 2024, pp. 130010, https://doi.org/10.1016/j.physleta.2024.130010.

[19] R. P. Singh, S. Yadav, D. Singh, G. Mishra, Theoretical Approach to Investigate Temperature Dependent Ultrasonic and Thermophysical Properties of Ti-Zr-Hf Ternary Alloy, Int. J. Res. Appl. Sci. Eng. Technol., Vol. 10, No. 11, 2022, pp. 583-588, https://doi.org/10.22214/ijraset.2022.47382.